Shedding Light on the Growth of Gold Nanoshells

Christian Sauerbeck,[†,§,⊥] Michael Haderlein,[†,⊥] Benedikt Schürer,[†,‡,§] Björn Braunschweig,[†,§] Wolfgang Peukert,[†,‡,§] and Robin N. Klupp Taylor[†,‡,§,*]

[†]Institute of Particle Technology (LFG), University of Erlangen-Nuremberg, Cauerstrasse 4, 91058 Erlangen, Germany, [‡]Cluster of Excellence—Engineering of Advanced Materials (EAM), University of Erlangen-Nuremberg, Nägelsbachstrasse 49b, 91052 Erlangen, Germany, and [§]Erlangen Graduate School in Advanced Optical Technologies (SAOT), University of Erlangen-Nuremberg, Paul-Gordan-Strasse 6, 91058 Erlangen, Germany. [⊥]C. Sauerbeck and M. Haderlein contributed equally.

ABSTRACT Nanostructured particles containing noble metals can have highly tunable localized surface plasmon resonances and are therefore of particular interest for numerous applications. Nanoshells comprising a dielectric core and gold or silver shell are a widely researched systems because of the strong dependence of their optical properties on the ratio of core diameter to shell thickness. Although seeded-growth procedures have been developed to produce these particles, the many reported studies show significant variation in the nanoshell morphologies and hence optical properties. In order to establish processes that reproducibly synthesize nanoshells with high optical quality, it is necessary to develop techniques that monitor changes at the core particle surface during shell growth. For that purpose, we have carried out *in situ* nonlinear second-harmonic scattering (SHS) and linear vis−NIR extinction spectroscopy simultaneously during the seeded growth of gold nanoshells on silica core particles. Our SHS measurements show a striking variation in the nonlinear optical properties of the growing gold nanoshells. In comparison with linear optical measurements and with scanning electron microscopy (SEM) images made of gold nanoshells produced with varying shell completenesses, the SHS signal was observed to reach a peak intensity at a stage prior to shell closure. We attribute this high sensitivity of the SHS signal to the incomplete nanoshell surface morphology to the generation and subsequent degeneration of regions of electric field enhancement at gaps between isolated gold islands, which grow and coalesce. This conclusion is corroborated by finite-difference time-domain simulations of incomplete nanoshells. We suggest that the *in situ* analytical approach demonstrated here offers significant promise for future activities regarding the in-process optimization of the morphology and optical properties of metal nanoshells and other nanostructured plasmonic particles.

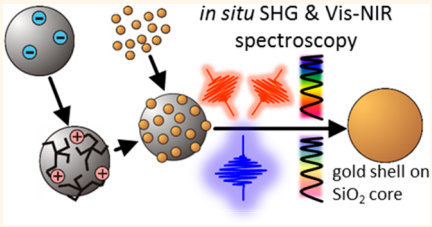

KEYWORDS: plasmonic particles · electric field enhancement · *in situ* vis−NIR spectroscopy · second-harmonic generation · nanostructured particles

There is currently considerable interest in the synthesis and application of particles with tunable optical properties based on the localized surface plasmon resonance (LSPR).[1−10] In particular, core−shell as well as hollow structures comprising gold or silver are intensively studied because of their highly structure-dependent resonances making them relevant for a range of photonic, optoelectronic, and biomedical applications.[11−16] Following the original work of Halas and co-workers to realize gold[17] and silver[18] nanoshells through seeded growth strategies, numerous reports on synthetic improvements,[19] structure−property relationships,[20] and possible applications of such particles have been published.[13,21] While synthetic metal nanoshells can have very striking optical properties, bearing close resemblance to the result of Lorenz−Mie simulations for perfectly spherical core−shell structures,[17] a large spread in the quality of results can be elucidated by careful analysis of the literature.[21−26] This is unsurprising since the typical synthesis of metal nanoshells comprises a multistep procedure including a core particle functionalization step, a seed nanoparticles adsorption step, and a seed nanoparticles ripening step. While the first two steps can lead to poor quality shells due to incomplete functionalization or seed adsorption, respectively, the latter step, being an electroless heterogeneous crystal growth reaction, is already known to be quite sensitive to various parameters including the age of the precursors and the type of reducing agent.[19,25] Nevertheless, to the best of our knowledge there have been no reported studies of the nanoshell growth step *in situ* and in real time using one or more techniques. Such an investigation would be of great importance since it would provide a

* Address correspondence to robin.klupp.taylor@fau.de.

Received for review February 6, 2014 and accepted February 19, 2014.

Published online February 19, 2014
10.1021/nn500729r

means to elucidate the influence of the process parameters on the intermediate structures formed and identify how these can go on to grow into complete nanoshells with high optical quality.

Microscopic methods such as transmission electron microscopy (TEM),[27,28] scanning electron microscopy (SEM),[29,30] and atomic force microscopy (AFM)[31] allow direct investigations of surface nanostructures with high spatial resolution. Additionally, methods such as photoelectron emission microscopy (PEEM)[32] are able to identify geometries with desired plasmonic properties. While these techniques can easily contribute to a characterization of surface structures *ex situ*,[13,20] *in situ* information is not readily attainable as shells are formed in aqueous suspension. Small angle X-ray scattering (SAXS) and small angle neutron scattering (SANS) can give information about particle size, shape, and surface structures.[33,34] While the *in situ* seeded growth of single phase gold particles has been successfully studied by SAXS,[35] the necessary increment in model complexity in order to represent the growth of many gold islands on a core particle surface is currently prohibitive.

Because of the striking optical properties of metal nanoshells, considerable effort has already been made to compare electrodynamic simulations to experimental results in order to characterize geometric data such as shell thickness.[36] However, only a few studies have closely considered the evolution of the optical properties of such particles going from the seeded core *via* an incomplete shell up to a complete shell. A significant challenge is the rationalization of the three overlaying effects, namely, the size increase of individual seed gold particles, the growing together of those seed particles to form islands with nonspherical shape, and the electrodynamic interactions between the growing gold islands. It is clear that numerical approaches are required, though as shown recently for a much simpler multicomponent plasmonic system, the inclusion of polydispersity, a feature of all real systems, can make the problem of reconstructing experimental data truly formidable.[37] To the best of our knowledge, the two most significant works are the experimental and theoretical study of Preston and Signorell[13] and the theoretical study of Peña-Rodríguez and Pal.[38] In the former case, discrete dipole approximation (DDA) simulations of interacting hemispherical gold islands accounted for the shifting and splitting of resonances seen during the shell growth. In the latter work, DDA and T-matrix simulations of incomplete nanoshells illustrated that potentially useful optical properties may actually be obtained by avoiding the formation of a complete shell, a conclusion which will be shared by the present work. These works underline the need for deeper experimental study involving more methods than are currently employed. For this purpose we propose to combine linear and nonlinear optical spectroscopic methods for the *in situ* study of gold nanoshells growth.

Second-harmonic generation (SHG) is a nonlinear optical process that is highly interface specific for materials with inversion symmetry such as liquids, gold, and silica. Second-harmonic light scattering (SHS) from interfaces of colloidal particles has thus become a versatile noninvasive tool to probe interfacial molecular structures[39−43] and to track surface processes at colloidal interfaces with high temporal resolution.[44−46] However, only a few experimental studies of the nonlinear optical properties of nanoshells exist,[31,47] and to the best of our knowledge *in situ* SHS studies during nanoshell growth are still missing. The latter would, however, increase our level of understanding considerably as SHS can provide a direct measure of local electric fields[48] and is thus a direct measure of surface structures with high plasmonic field enhancements.[49]

In this work we have carried out synchronous *in situ* SHS and vis−NIR extinction spectroscopy during the formation of high quality gold nanoshells on colloidal silica particles. Characteristic features relating to the different stages of growth were observed in the SHS measurement and enabled us to deliberately produce incomplete shells with maximized second harmonic generation capability. Our measurements reveal that *in situ* nonlinear optical characterization approaches may offer greater possibilities for the monitoring and optimization of the synthesis of nanoshells with high quality linear optical properties and other tailored metal nanostructures for certain applications.

RESULTS AND DISCUSSION

The seeded growth method to produce gold nanoshells on silica cores was first reported by Oldenburg *et al.*[17] In this, small gold nanoparticles, produced *via* the route reported by Duff,[50] are adsorbed to amine-functionalized silica particles and are ripened by formaldehyde reduction of a dark-aged solution of chloroauric acid and potassium carbonate (the latter being referred to here as k-gold). Using the same approach to produce gold shells on 210 ± 9 nm diameter silica cores, we carried out a systematic *in situ* study of the linear and nonlinear optical properties during the nanoshell growth. In a first step we determined the necessary reaction conditions, *i.e.*, seed, k-gold, and formaldehyde concentration, to produce complete gold shells with a high quality optical extinction spectrum, *i.e.*, one that can be reproduced by Lorenz−Mie simulations. These conditions were then used in our initial *in situ* simultaneous linear and nonlinear optical study of the growing shell (Figure 1a,f,k). Figure 1a shows a representative SEM image of the final product, while Figure S1a (Supporting Information) shows a wider view, confirming the regularity of the particles produced. The temporal evolution of the optical extinction spectrum during shell growth is presented in Figure 1f. A continuous increase in extinction with reaction time was found across the investigated

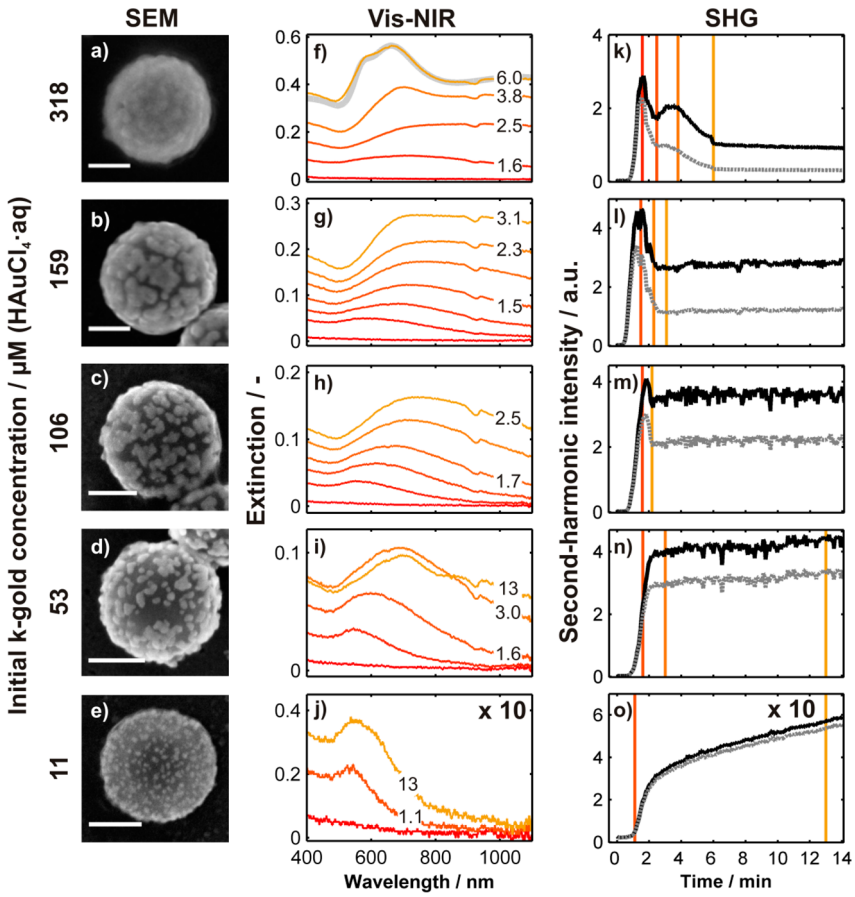

Figure 1. Seeded growth of gold nanoshells on silica core particles studied by SEM, *in situ* vis−NIR extinction spectroscopy and *in situ* second-harmonic scattering (SHS). The final gold coverage was adjusted by the initial concentration of k-gold as indicated. (a−e) Representative SEM images of the products. Scale bars correspond to 100 nm. (f−j) Evolution of extinction spectra for selected time steps (in minutes) during the shell growth reaction. The gray spectrum in (f) corresponds to the best match Lorenz−Mie simulation of a spherical nanoshell. (k−o) Changes in SHS intensity during the reaction measured at a scattering angle θ of 20°. Gray lines show the as-measured SHS intensity. Black lines are corrected for losses on the basis of the extinction data (see Experimental Details). Vertical guidelines correspond to the times indicated in the extinction spectra.

wavelength range. For reasons of clarity the number of spectra shown in Figure 1f has been limited, the time of acquisition for each spectrum being noted on the right-hand side. Corresponding *in situ* extinction data with a higher temporal resolution are shown in Figure S2 (Supporting Information). During early stages of shell growth (up to around 1.6 min) a feature at around 550 nm arises in the extinction spectra. This can be attributed to the plasmon resonance of noncontiguous gold nanoparticle assemblies with a limited degree of plasmonic intercoupling.[13,51] As growth time progresses (up to around 2.5 min), the spectral feature red shifts and broadens, corresponding to both the increasing size and plasmonic intercoupling of the gold particles on the silica surface. At the final stages of shell growth at around 6 min, which was identified as the time after which the spectrum ceased to change further, a blue shift and emergence of a peak at 680 nm, and later, a shoulder at 590 nm can be seen. A very broad feature centered at around 1000 nm is also observed. This behavior is consistent with *ex situ* measurements of Oldenburg *et al.*,[17] Preston and Signorell,[13] and others and results from the fusion of gold islands on the silica surface to produce shells that are capable of supporting higher frequency (shorter wavelength) optical resonances than the structures present in the incomplete shells. To confirm that gold nanoshells were successfully produced, we carried out simulations based on an extended Lorenz−Mie approach, which includes the possibility to incorporate polydispersity in the core diameter and shell thickness.[52] To simulate a spectrum closely matching the final spectrum of our *in situ* study (Figure 1f, gray line) we used a mean and standard deviation core diameter of 210 and 9 nm, respectively, and a mean and standard deviation shell thickness of 38 and 7 nm, respectively. Only the mean shell thickness was adjusted during matching of the experimental and theoretical spectra since all other parameters were determined by image analysis of SEM micrographs (Figure S3, Supporting Information). Figure S4 (Supporting Information) also demonstrates that the inclusion of polydispersity in the core diameter and shell thickness only serves to broaden the features of the spectrum but does not shift them.

We point out that there is excellent agreement between the extinction spectra of Lorenz−Mie simulations and from our experimental results (see Figure 1f). For that reason, it is possible to conclude that in our experiments high quality gold nanoshells were produced, because smooth and closed shells are prerequisite for the application of a Lorenz−Mie approach. In addition, our approach does also allow the attribution of the features at 590, 680, and 1000 nm to octupole, quadrupole and dipole resonances of the gold shells, respectively. The differences between the spectra most likely arise from the fact that the produced shells are rough and contain some defects such as crevices between parts of the shell that have not closed during the growth (see Figure S1a, Supporting Information).

Simultaneous with the *in situ* extinction measurements of the growing gold shell (Figure 1f), we also measured the evolution of SHS intensities at a scattering angle of 20° for p-in and p-out polarizations (Figure 1k). To aid the comparison of the figures, vertical lines are shown in Figure 1k at times corresponding to the acquisition of the spectra shown in Figure 1f. In addition to the raw SHS data (gray lines), we also show corrected data (black lines). The latter accounts for changes in SHS intensities due to the increased extinction at the fundamental as well as second-harmonic wavelengths (see the Experimental Details). The SHS intensity during gold shell growth initially shows a steep increase to a maximum of 2.9 au after 1.6 min. This maximum is subsequently followed by a sharp decrease in intensity up to 2.5 min followed by an increase to about 2.1 au at about 3.8 min. Following this, the SHS intensity decreases until it becomes constant at around 1.2 au after about 6 min. Since this time also corresponds to the point when the extinction spectra (Figure 1f) ceases to change, we can infer that the gold precursor has been consumed and the reaction has stopped. We were able to reproduce the general trend in SHS intensity characterized by a steep increase followed by a decline several times. However, the second maximum that is observed after 3.8 min in Figure 1k was not present in all experiments at the high k-gold concentrations used. Figure S5 (Supporting Information) provides an example for such a case, and comparison of the corresponding extinction spectra with Figure 1f suggest that the quality of the final shells produced in Figure S5 (Supporting Information) is inferior. This may therefore explain the absence of the additional peak in the second-harmonic (SH) signal during growth of those nanoshells.

The fact that such strong features in the SHS signal shown in Figure 1k arose during nanoshell growth is rather surprising and cannot be inferred from the linear extinction spectra, which show rather gradual changes to their broad features. This result suggests that at intermediate stages of shell growth, morphologies capable of generating significantly higher SHS signals than complete nanoshells are being produced. To gain a deeper understanding of the incomplete shell structures that are contributing to this phenomenon, we performed experiments wherein the shell growth reaction was adjusted in order that it ceased at intermediate stages of growth. We achieved this by reducing the initial concentration of k-gold in the growth solution while maintaining the overall volume constant (see Table 1). In Figure 1, the results of four different *in situ* studies of incomplete nanoshells growth are compared to the data for the growth of complete nanoshells already discussed above. The presentation of all data, including selection of representative extinction spectra for clarity, has been carried out in exactly the same way as for the data of Figure 1a, f,k. The representative SEM images (Figure 1b−e) are again supported by larger area micrographs (Figure S1b−e, Supporting Information). Consistent with the work of Oldenburg *et al.*,[17] our SEM images show that as the concentration of k-gold increases, separated gold seed particles grow in size and form islands that eventually coalesce into complete Au shells with a certain degree of surface roughness. A comparison of the *in situ* optical extinction data for different k-gold concentrations (Figure 1f−j) indicates that in general the temporal evolution is consistent and points to a growth reaction mechanism that is independent of the k-gold concentration. This is despite the fact that, as can be seen from the times of the final spectra shown, lower k-gold concentration generally leads to a much slower reaction.

Figure 1k−o compares the *in situ* measured SHS intensities for the gold shell growth reactions with different concentrations of k-gold. In all cases, the SHS intensity is seen to increase rapidly within the first two minutes of the reaction, consistent with the observation we already made for the growth of the complete gold shells (Figure 1k). For k-gold concentrations of 318, 159, and 106 μM (Figure 1k−m) the SHS intensity traces out at least one peak and remains constant when the reaction is finished. Differences in absolute SHS peak intensities are attributed to small variations of the particle concentration for each experiment. However, the ratio between the peak intensity and the final value can be compared between the different reactions and is seen to clearly decrease as the initial concentration of k-gold and thus the final gold coverage is decreased. This confirms that by reducing the concentration of k-gold in the reaction, we can approach an incomplete shell structure that is close to that which produces the peak SHS signal. Indeed, for an initial concentration of 53 μM k-gold (Figure 1n) the reaction has clearly reached completion before or at the state of maximum SHS intensity, and

TABLE 1. Reactant Composition for the Synthesis of Gold Nanoshells with Varying Surface Coverage[a]

sample	volume of seeds (μL)	volume of k-gold (μL)	volume of CH_2O (μL)	volume of H_2O (μL)	concentration of k-gold ($HAuCl_4$ aq) (μM)
a	20	1500	250	0	318
b	20	750	250	750	159
c	20	500	250	1000	106
d	20	250	250	1250	53
e	20	50	250	1450	11

[a] The sample names correspond to the SEM images in Figure 1.

the SHS signal levels off following its initial increase. Finally, at 11 μM k-gold it can be seen that both vis−NIR extinction and SHS intensity (Figure 1e,o respectively) continuously increase during the entire course of the experiment indicating a very slow growth reaction.

Considering the clear evidence that a maximum in final SHS intensities will be generated when the reaction uses a k-gold concentration between 53 and 106 μM, we can identify from the SEM images corresponding to these limits (Figure 1c,d) the surface morphology that produces such a strong SHS response. In particular, gold islands with rather small separation can be seen in Figure 1d (53 μM k-gold), while these appear to have mostly coalesced to form larger surface structures in Figure 1c (106 μM k-gold). We therefore suggest that the growth and coalescence of these islands leads to the peak in the time evolution of SHS intensities through the generation of a strong local field enhancement.

Canfield *et al.*[53] studied the SHG signal arising from field enhancement in the gaps between orthogonally arranged gold nanobars. It was found that for relatively large gap sizes the field enhancement was nearly constant, while for small gap sizes it increased. Interestingly, the strongest SHG response was found for a gap size of zero and an anisotropic T-shaped structure. The field enhancement of irregular shaped gold nanostars was investigated by Hrelescu *et al.*[32] In their PEEM study they find local plasmonic hot spots at the tips of gold nanostars, which can be selectively excited by the appropriated polarization and wavelength of the excitation light. McMahon *et al.*[54] investigated the effect of small gaps for different geometries on the local electric field and its influence on surface-enhanced Raman spectroscopy (SERS). In contrast to Canfield *et al.*, they found a maximum enhancement inside the gaps. In the present study, the structure of gold islands on colloidal silica cores that give rise to the highest SHS intensities are characterized by both irregular shape and gaps between individual islands (see Figure 1c,d). Therefore, in view of the related literature, it is reasonable to attribute the strong SHS responses observed to a local field enhancement in the cavities between individual gold nanoislands. This interpretation is further backed up by Anceau *et al.* who investigated the effect of local field enhancement at nanostructured gold coatings on planar silica substrate by SHG microscopy.[49] It was demonstrated that the signal obtained from this technique is highly sensitive to the morphology of the gold surface. During the formation of the gold nanoshells in colloidal suspension the situation is not that different from the one described by Anceau and co-workers. As the gold nanoparticles grow on the silica surface, gaps between the initially separate islands form, and plasmonic coupling across these gaps enhance the fundamental field in or near them. Since the second-harmonic field scales with the square of the fundamental field intensity, a strong enhancement of the fundamental field will be associated with a commensurate strong increase of SHS intensity. In the course of the shell growth reaction, islands coalesce and form complete shells. Consequently, the gaps between gold islands disappear and cause a subsequent decrease in local field enhancement that is accompanied by substantial decrease in overall SH intensity. However, as indicated by the SEM images in Figure 1a and Figure S1a (Supporting Information), this reaction leads to gold shells that are not perfectly smooth but have a certain surface roughness. Lowering the initial concentration of k-gold (Figure 1b and Figure S1b, Supporting Information) results in more open shell structures where silica cores are covered by large islands separated by wide gaps. These islands show a 3D growth and thus can create deep crevices between them immediately before they coalesce and form a closed shell. From the study of planar metallic, *e.g.*, silver or gold, interfaces it is known that in contrast to smooth substrates, rough surfaces can give rise to an enhancement of SHG signals by up to 4 orders of magnitude.[55] Therefore we suggest that the second, lower SHS peak measured during complete gold shell growth at around 3.8 min (see Figure 1k) can be attributed to enhancement in crevices between large coalescing gold islands in the final stage of the shell growth. In the further course of the reaction (3.8−6 min in Figure 1k), these crevices will be filled up resulting in a decrease in local field enhancement and thus SHS intensity.

In order to corroborate our conclusion that the gaps between gold islands and therefore the surface morphology of incomplete nanoshells can lead to strong field enhancements, we performed simulations of the electric field for different surface structures. Simulations were performed by the commercial software

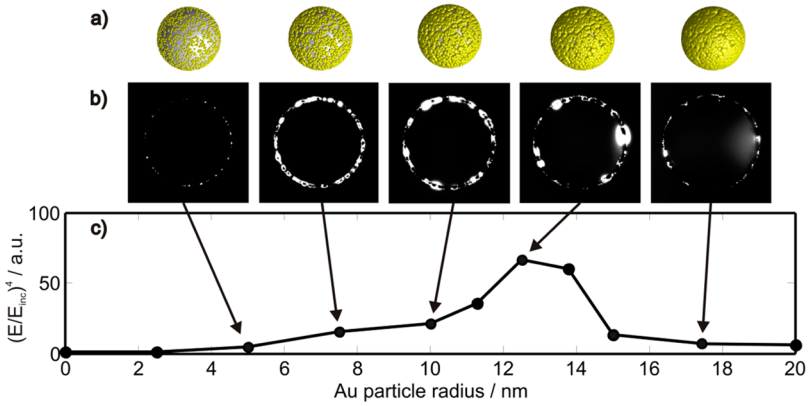

Figure 2. (a) Illustration of silica−gold core shell structures used in FDTD simulations that comprise a 300 nm silica core and Au hemispheres with 5, 7.5, 10, 12.5, and 17.5 nm radii (left to right). (b) Visualization of the fourth power of the simulated relative local electric field $(E/E_{inc})^4$ over the cross section of the particle. (c) Plot of the fourth power of the local relative electric field integrated over the simulated particles' surface *versus* the radius of the gold hemispheres at the silica surface. The line is included as a guide to the eye.

FDTD solutions (Lumerical Solutions, Inc.), which solves Maxwell's equations based on the finite-difference time-domain (FDTD) method on 3D geometries. The geometry used for our simulations was composed of a single silica sphere covered by a large number (2000) of randomly distributed gold hemispheres. The latter morphology of gold islands was selected, partly because of the proven success of the assumption in a previous report[13] and also because of the fact that TEM studies of gold islands on particles with similar functionality have been observed to wet the core particle surface rather than form spheroidal particles.[56]

The number of hemispheres was chosen to mimic a situation with a large number of individual particles with a small size that is similar to the experimentally observed situation as shown in Figure 1e. While both size of the silica sphere and position of gold hemispheres were fixed for each simulation, the size of each gold hemisphere was varied, resulting in different degrees of coverage. Figure 2a presents the geometrical assemblies of some silica core and gold hemispheres that have been used in our simulations.

Results of our FDTD simulations are shown in Figure 2b,c. As the experimentally measured SHS intensity scales with the fourth power of the fundamental electric field, we present in Figure 2b a cross-section through the particle showing the fourth power of the local electric field at an excitation wavelength of 800 nm. Bright areas correspond to a strong field enhancement. Although this visual comparison is qualitative, it is clear that for the case of 10 and 12.5 nm hemisphere radii, hot spots and thus large local values for $(E/E_{inc})^4$ can be observed. However, both lower and higher degrees of coverage appear to lead to rather lower field enhancements. Figure 2c presents the fourth power of the relative electric field integrated over the entire surface as a function of gold nanoparticle radii. A clear increase and then decrease of $(E/E_{inc})^4$ can be observed. In particular, the peak in $(E/E_{inc})^4$ appears to be close to where gold hemispheres coalesce together. This trend is therefore consistent with our *in situ* measurements of SHS from growing gold shells as well as our interpretation regarding the generation of local field enhancement. However, whether individual hot spots can dominate SHS signals or not is not obtainable by this rather qualitative comparison of simulations and experiments. As strong local fields at certain locations can give rise to local SH signals, it is likely that similar signals from the opposite side of the core particle are out-of-phase and hence interfere destructively. Therefore we expect that our SH measurements underestimate the actual field enhancement at the particle surface. The strength of this effect will depend on the ratio of particle size, shape, and wavelength as described by Wang *et al.*[57]

CONCLUSION

In conclusion, the seeded growth of gold nanoshells on silica cores in colloidal suspension has been studied *in situ* by simultaneous second-harmonic light scattering (SHS) and extinction spectroscopy. During shell growth, SHS intensities reached a maximum at an intermediate reaction stage where incomplete shell structures comprising gold islands covering the silica cores were observed. This intermediate maximum was followed by a substantial decrease in SHS intensity when closed shells were formed. FDTD simulations indicated a strong enhancement of local electric fields when the gold shell was incomplete and presented gaps between individual metal islands. As the SHS intensity depends on the fourth power of the fundamental electric field, we attribute the time evolution of SHS intensities during the shell growth to a generation and subsequent "growing out" of surface sites with strong local field enhancements. To the best of our knowledge this is the first time that an evolving property of plasmonic particles resulting from strong electromagnetic field enhancement has been studied

in situ during particle synthesis. We expect that application of the analytical approaches introduced here will lead to substantial improvements in control over synthesis conditions and final product properties for a wide range of similar reactions as well as self-assembly processes and thus contribute to the optimization of procedures for the fabrication of nanostructures with enhanced properties.

EXPERIMENTAL DETAILS

Gold Nanoshell Synthesis. For the formation of gold nanoshells we used a procedure similar to that of Oldenburg *et al.*[17] In the present work, only the final shell growth step of the synthesis was examined. The preceding steps comprise the synthesis of silica particles with a diameter of 210 nm according to the method of Stöber[58] followed by functionalization with an organosilane (3-aminopropyltriethoxysilane, Sigma-Aldrich, ≥98%). The latter treatment results in a reversal of surface charge and thus provides silica particles with a zeta potential of about +66 mV (Zetasizer Nano ZS, Malvern Instruments, UK). The amine functionality enables, in the following step, negatively charged gold nanoparticles synthesized according to the method described by Duff *et al.*[59] with an average diameter of about 2 nm to be attached to the surface of the silica. Nonadsorbed gold nanoparticles were removed in multiple cycles of centrifugation (10 min at 5000 rcf), decantation and redispersion. Although only the gold nanoparticles attached to the surface are believed to provide metal growth sites, in the following the whole gold nanoparticle decorated silica particles are referred to as the seed. Ripening of the seed into gold nanoshells was achieved by mixing them with a dark-aged solution of chloroauric acid (375 μM, Gold(III) chloride hydrate, Sigma-Aldrich) and potassium carbonate (1.8 mM, Carl Roth) (referred to as k-gold). The shell growth reaction was initiated by adding 3.7% formaldehyde solution (Carl Roth, diluted from a 37% solution with ultrapure water) as a reducing agent under rapid stirring. The diluted formaldehyde avoids the generation of high local concentrations of formaldehyde causing inhomogeneous reaction conditions. For different degrees of gold coverage the concentration of k-gold was varied, while the total reaction volume and the particle concentration, respectively, were kept constant by adding water. The composition of the different reactant solutions can be found in Table 1. Herein the maximum concentration of k-gold (318 μM) results in a complete gold shell, whereas for smaller concentration incomplete gold coverage is obtained.

***In Situ* SHS/Linear Extinction Measurements.** The setup used for the *in situ* SH scattering and linear vis−NIR extinction measurements has been described in detail previously.[60] SHS experiments were performed with a Ti:Sapphire laser (Tsunami, Spectra-Physics) operated at a wavelength of 800 nm and 80 fs pulse duration. The polarization of the laser beam was adjusted with a half-wave plate (Thorlabs, AQWP05M-980). The beam was focused by a lens (f = 50 mm) into the center of a cylindrical quartz glass cuvette with an inner diameter of 8 mm. A small magnetic stir bar (7 × 2 mm) was used to provide homogeneous reaction conditions inside the cuvette as well as to prevent sedimentation. After passing the sample, scattered light was led through a set of spectral filters (Schott, BG39; L.O.T.-ORIEL, ET402/15X) and a Glan-Laser polarizer (Thorlabs, GL5-A) in order to selectively detect SH light of a specified polarization. The SH light was detected by a photomultiplier tube (Hamamatsu, R7205-1) and recorded by a photon counting unit (Hamamatsu, C3866). Optical filters and photomultiplier tube were mounted to a motorized goniometer stage. This setup allows for a detection of SH light at well-defined angular positions. In order to increase angular resolution SHS signals were detected from solid angle of 3°, only which was achieved by the integration of a suitable aperture. The SH signals were averaged over 50 subsequent measurements where each measurement had an acquisition time of 50 ms. A fiber coupled light source (Ocean Optics, DH-200-BAL) powering a vis−NIR spectrometer (Avantes, AvaSpec-ULS3648) allowed the acquisition of the extinction spectrum synchronized with the SHG signal. The combination of both techniques allowed for a temporal resolution in the range of seconds. Besides providing additional linear spectroscopic information, the *in situ* measured extinction spectrum enables an important correction of the SH signal. It has been shown previously that the SH intensity depends not only on the properties of the interfacial layer of colloidal particles, but also on effects of linear light scattering and absorption.[61,60] In other words, photons of the fundamental laser beam are absorbed or scattered on their way to the focal volume before being able to generate SH photons. Similarly, SH photons are absorbed or scattered on their way to the detector. In the present case the optical density remains in a regime describable by Lambert's law. Thus, by tracking the optical density by extinction spectroscopy during the growth and under the assumption that SHG essentially takes place in the focal region in the center of the cuvette, the influence of the linear optical properties can be corrected by eq 1:

$$I_{2\omega} = I_{2\omega,\,\mathrm{det}} \cdot \exp\left(E_{800\mathrm{nm}} + \frac{1}{2}E_{400\mathrm{nm}}\right) \qquad (1)$$

Here, $I_{2\omega,\mathrm{det}}$ is the detected SH intensity, $I_{2\omega}$ is the corrected SH intensity, and E_λ is the extinction at either the fundamental or the second-harmonic wavelength. In order to maintain the validity of the correction described in eq 1 and to limit the heat input by the laser beam, the *in situ* gold nanoshell synthesis was carried out under diluted conditions compared to the original recipe described by Oldenburg.[17]

***Ex Situ* Characterization.** SEM pictures of the final products were recorded with a Zeiss Gemini Ultra 55 field emission scanning electron microscope.

Conflict of Interest: The authors declare no competing financial interest.

Acknowledgment. The authors gratefully acknowledge the funding by the German National Science Foundation through Project PE 427/11 and support by the Erlangen Graduate School in Advanced Optical Technologies (SAOT) and the Cluster of Excellence "Engineering of Advanced Materials" at the University of Erlangen-Nuremberg, within the framework of the "Excellence Initiative"

Supporting Information Available: SEM overview images, *in situ* vis−NIR at high temporal resolution, particle size distributions, Lorenz−Mie simulations, additional *in situ* extinction and SHG data, and second-harmonic scattering profiles. This material is available free of charge *via* the Internet at http://pubs.acs.org.

REFERENCES AND NOTES

1. Stewart, M. E.; Anderton, C. R.; Thompson, L. B.; Maria, J.; Gray, S. K.; Rogers, J. A.; Nuzzo, R. G. Nanostructured Plasmonic Sensors. *Chem. Rev.* **2008**, *108*, 494–521.
2. Anker, J. N.; Hall, W. P.; Lyandres, O.; Shah, N. C.; Zhao, J.; van Duyne, R. P. Biosensing with Plasmonic Nanosensors. *Nat. Mater.* **2008**, *7*, 442–453.
3. Lu, X.; Rycenga, M.; Skrabalak, S. E.; Wiley, B.; Xia, Y. Chemical Synthesis of Novel Plasmonic Nanoparticles. *Annu. Rev. Phys. Chem.* **2009**, *60*, 167–192.
4. Sau, T. K.; Rogach, A. L.; Jäckel, F.; Klar, T. A.; Feldmann, J. Properties and Applications of Colloidal Nonspherical Noble Metal Nanoparticles. *Adv. Mater.* **2010**, *22*, 1805–1825.
5. Mayer, K. M.; Hafner, J. H. Localized Surface Plasmon Resonance Sensors. *Chem. Rev.* **2011**, *111*, 3828–3857.
6. Cobley, C. M.; Chen, J.; Cho, E. C.; Wang, L. V.; Xia, Y. Gold Nanostructures: A Class of Multifunctional Materials for Biomedical Applications. *Chem. Soc. Rev.* **2011**, *40*, 44–56.

7. Li, C.; Sun, L.; Sun, Y.; Teranishi, T. One-pot Controllable Synthesis of Au@Ag Heterogeneous Nanorods with Highly Tunable Plasmonic Absorption. *Chem. Mater.* **2013**, *25*, 2580–2590.
8. Knight, M. W.; King, N. S.; Liu, L.; Everitt, H. O.; Nordlander, P.; Halas, N. J. Aluminum for Plasmonics. *ACS Nano* **2013**, *8*, 834–840.
9. Fong, K. E.; Yung, L.-Y. L. Localized Surface Plasmon Resonance: A Unique Property of Plasmonic Nanoparticles for Nucleic Acid Detection. *Nanoscale* **2013**, *5*, 12043–12071.
10. Bansal, A.; Sekhon, J.; Verma, S. S. Scattering Efficiency and LSPR Tunability of Bimetallic Ag, Au, and Cu Nanoparticles. *Plasmonics* **2013**, 1–8.
11. Hirsch, L. R.; Stafford, R. J.; Bankson, J. A.; Sershen, S. R.; Rivera, B.; Price, R. E.; Hazle, J. D.; Halas, N. J.; West, J. L. Nanoshell-Mediated Near-Infrared Thermal Therapy of Tumors under Magnetic Resonance Guidance. *Proc. Natl. Acad. Sci. U. S. A.* **2003**, *100*, 13549–13554.
12. Xu, Z.; Hou, Y.; Sun, S. Magnetic Core/Shell Fe3O4/Au and Fe3O4/Au/Ag Nanoparticles with Tunable Plasmonic Properties. *J. Am. Chem. Soc.* **2007**, *129*, 8698–8699.
13. Preston, T. C.; Signorell, R. Growth and Optical Properties of Gold Nanoshells Prior to the Formation of a Continuous Metallic Layer. *ACS Nano* **2009**, *3*, 3696–3706.
14. Cortie, M. B.; McDonagh, A. M. Synthesis and Optical Properties of Hybrid and Alloy Plasmonic Nanoparticles. *Chem. Rev.* **2011**, *111*, 3713–3735.
15. Jankiewicz, B. J.; Jamiola, D.; Choma, J.; Jaroniec, M. Silica–Metal Core–Shell Nanostructures. *Adv. Colloid Interface Sci.* **2012**, *170*, 28–47.
16. Hu, T.; Lin, Y.; Yan, J.; Di, J. Synthesis of Hollow Gold Nanoparticles on the Surface of Indium Tin Oxide Glass and their Application for Plasmonic Biosensor. *Spectrochim. Acta, Part A* **2013**, *110*, 72–77.
17. Oldenburg, S. J.; Averitt, R. D.; Westcott, S. L.; Halas, N. J. Nanoengineering of Optical Resonances. *Chem. Phys. Lett.* **1998**, *288*, 243–247.
18. Jackson, J. B.; Halas, N. J. Silver Nanoshells: Variations in Morphologies and Optical Properties. *J. Phys. Chem. B* **2001**, *105*, 2743–2746.
19. Brinson, B. E.; Lassiter, J. B.; Levin, C. S.; Bardhan, R.; Mirin, N.; Halas, N. J. Nanoshells Made Easy: Improving Au Layer Growth on Nanoparticle Surfaces. *Langmuir* **2008**, *24*, 14166–14171.
20. Wang, H.; Goodrich, G. P.; Tam, F.; Oubre, C.; Nordlander, P.; Halas, N. J. Controlled Texturing Modifies the Surface Topography and Plasmonic Properties of Au Nanoshells. *J. Phys. Chem. B* **2005**, *109*, 11083–11087.
21. Kah, J. C. Y.; Phonthammachai, N.; Wan, R. C. Y.; Song, J.; White, T.; Ahmad, I.; Sheppard, C.; Olivo, M. Synthesis of Gold Nanoshells Based on the Deposition-Precipitation Process. *Gold Bull.* **2008**, *41*, 23–36.
22. Ji, T.; Lirtsman, V. G.; Avny, Y.; Davidov, D. Preparation, Characterization, and Application of Au-Shell/Polystyrene Beads and Au-Shell/Magnetic Beads. *Adv. Mater.* **2001**, *13*, 1253–1256.
23. Graf, C.; van Blaaderen, A. Metallodielectric Colloidal Core-Shell Particles for Photonic Applications. *Langmuir* **2002**, *18*, 524–534.
24. Shi, W.; Sahoo, Y.; Swihart, M. T.; Prasad, P. N. Gold Nanoshells on Polystyrene Cores for Control of Surface Plasmon Resonance. *Langmuir* **2005**, *21*, 1610–1617.
25. Liang, Z.; Liu, Y.; Ng, S. S.; Li, X.; Lai, L.; Luo, S.; Liu, S. The Effect of pH Value on the Formation of Gold Nanoshells. *J. Nanopart. Res.* **2011**, *13*, 3301–3311.
26. Gomez, L.; Arruebo, M.; Sebastian, V.; Gutierrez, L.; Santamaria, J. Facile Synthesis of SiO2-Au Nanoshells in a Three-Stage Microfluidic System. *J. Mater. Chem.* **2012**, *22*, 21420–21425.
27. Yong, K.-T.; Sahoo, Y.; Swihart, M. T.; Prasad, P. N. Synthesis and Plasmonic Properties of Silver and Gold Nanoshells on Polystyrene Cores of Different Size and of Gold-Silver Core-Shell Nanostructures. *Colloids Surf., A* **2006**, *290*, 89–105.
28. Klupp Taylor, R. N.; Bao, H.; Tian, C.; Vasylyev, S.; Peukert, W. Facile Route to Morphologically Tailored Silver Patches on Colloidal Particles. *Langmuir* **2010**, *26*, 13564–13571.
29. Bao, H.; Peukert, W.; Taylor, R. N. K. One-Pot Colloidal Synthesis of Plasmonic Patchy Particles. *Adv. Mater.* **2011**, *23*, 2644–2649.
30. Hanisch, M.; Maković, M.; Taccardi, N.; Spiecker, E.; Klupp Taylor, R. N. Synthesis of Silver Nanoparticle Necklaces Without Explicit Addition of Reducing or Templating Agents. *Chem. Commun.* **2012**, *48*, 4287–4289.
31. Ros, I.; Schiavuta, P.; Bello, V.; Mattei, G.; Bozio, R. Femtosecond Nonlinear Absorption of Gold Nanoshells at Surface Plasmon Resonance. *Phys. Chem. Chem. Phys.* **2010**, *12*, 13692–13698.
32. Hrelescu, C.; Sau, T. K.; Rogach, A. L.; Jäckel, F.; Laurent, G.; Douillard, L.; Charra, F. Selective Excitation of Individual Plasmonic Hotspots at the Tips of Single Gold Nanostars. *Nano Lett.* **2011**, *11*, 402–407.
33. Fischer, B.; Autenrieth, T.; Wagner, J. Highly Charged Inorganic–Organic Colloidal Core–Shell Particles. *Langmuir* **2010**, *26*, 6201–6205.
34. Subramanian, N. D.; Moreno, J.; Spivey, J. J.; Kumar, C. S. S. R. Copper Core–Porous Manganese Oxide Shell Nanoparticles. *J. Phys. Chem. C* **2011**, *115*, 14500–14506.
35. Polte, J.; aHerder, M.; Erler, R.; Rolf, S.; Fischer, A.; Würth, C.; Thünemann, A. F.; Kraehnert, R.; Emmerling, F. Mechanistic Insights Into Seeded Growth Processes of Gold Nanoparticles. *Nanoscale* **2010**, *2*, 2463–2469.
36. Jain, P. K.; Lee, K. S.; El-Sayed, I. H.; El-Sayed, M. A. Calculated Absorption and Scattering Properties of Gold Nanoparticles of Different Size, Shape, and Composition: Applications in Biological Imaging and Biomedicine. *J. Phys. Chem. B* **2006**, *110*, 7238–7248.
37. Gudjonson, H.; Kats, M. A.; Liu, K.; Nie, Z.; Kumacheva, E.; Capasso, F. Accounting for Inhomogeneous Broadening in Nano-optics by Electromagnetic Modeling Based on Monte Carlo Methods. *Proc. Natl. Acad. Sci. U. S. A.* **2014**, 10.1073/pnas.1323392111.
38. Peña-Rodríguez, O.; Pal, U. Enhanced Plasmonic Behavior of Incomplete Nanoshells: Effect of Local Field Irregularities on the Far-Field Optical Response. *J. Phys. Chem. C* **2011**, *115*, 22271–22275.
39. Yan, E. C. Y.; Liu, Y.; Eisenthal, K. B. New Method for Determination of Surface Potential of Microscopic Particles by Second Harmonic Generation. *J. Phys. Chem. B* **1998**, *102*, 6331–6336.
40. Schürer, B.; Peukert, W. *In Situ* Surface Characterization of Polydisperse Colloidal Particles by Second Harmonic Generation. *Part. Sci. Technol.* **2010**, *28*, 458–471.
41. Haber, L. H.; Kwok, S. J. J.; Semeraro, M.; Eisenthal, K. B. Probing the Colloidal Gold Nanoparticle/Aqueous Interface with Second Harmonic Generation. *Chem. Phys. Lett.* **2011**, *507*, 11–14.
42. Schürer, B.; Hoffmann, M.; Wunderlich, S.; Harnau, L.; Peschel, U.; Ballauff, M.; Peukert, W. Second Harmonic Light Scattering from Spherical Polyelectrolyte Brushes. *J. Phys. Chem. C* **2011**, *115*, 18302–18309.
43. Butet, J.; Russier-Antoine, I.; Jonin, C.; Lascoux, N.; Benichou, E.; Brevet, P. F. Effect of the Dielectric Core and Embedding Medium on the Second Harmonic Generation from Plasmonic Nanoshells: Tunability and Sensing. *J. Phys. Chem. C* **2013**, *117*, 1172–1177.
44. Eckenrode, H. M.; Jen, S. H.; Han, J.; Yeh, A. G.; Dai, H.-L. Adsorption of a Cationic Dye Molecule on Polystyrene Microspheres in Colloids: Effects of Surface Charge and Composition Probed by Second Harmonic Generation. *J. Phys. Chem. B* **2005**, *109*, 4646–4653.
45. You, Y.; Bloomfield, A.; Liu, J.; Fu, L.; Herzon, S. B.; Yan, E. C. Y. Real-Time Kinetics of Surfactant Molecule Transfer Between Emulsion Particles Probed by *In Situ* Second Harmonic Generation Spectroscopy. *J. Am. Chem. Soc.* **2012**, *134*, 4264–4268.
46. Haber, L. H.; Eisenthal, K. B. Molecular Excited-State Relaxation Dynamics at the Colloidal Microparticle Interface

Monitored with Pump-Probe Second Harmonic Generation. *J. Phys. Chem. B* **2013**, *117*, 4249–4253.
47. Wu, D. J.; Liu, X. J.; Liu, L. L.; Qian, W. P. Third-Order Nonlinear Optical Properties of Gold Nanoshells in Aqueous Solution. *Appl. Phys. A: Mater. Sci. Process.* **2008**, *92*, 279–282.
48. Wunderlich, S.; Peschel, U. Plasmonic Enhancement of Second Harmonic Generation on Metal Coated Nanoparticles. *Opt. Express* **2013**, *21*, 18611–18623.
49. Anceau, C.; Brasselet, S.; Zyss, J.; Gadenne, P. Local Second-Harmonic Generation Enhancement on Gold Nanostructures Probed by Two-Photon Microscopy. *Opt. Lett.* **2003**, *28*, 713–715.
50. Duff, D. G.; Baiker, A.; Edwards, P. P. A New Hydrosol of Gold Clusters. 1. Formation and Particle Size Variation. *Langmuir* **1993**, *9*, 2301–2309.
51. Storhoff, J. J.; Lazarides, A. A.; Mucic, R. C.; Mirkin, C. A.; Letsinger, R. L.; Schatz, G. C. What Controls the Optical Properties of DNA-Linked Gold Nanoparticle Assemblies? *J. Am. Chem. Soc.* **2000**, *122*, 4640–4650.
52. Peña-Rodríguez, O.; González Pérez, P. P.; Pal, U. MieLab: A Software Tool to Perform Calculations on the Scattering of Electromagnetic Waves by Multilayered Spheres. *Int. J. Spectrosc.* **2011**, *2011*, 583743-1–583743-10.
53. Canfield, B. K.; Husu, H.; Laukkanen, J.; Bai, B.; Kuittinen, M.; Turunen, J.; Kauranen, M. Local Field Asymmetry Drives Second-Harmonic Generation in Noncentrosymmetric Nanodimers. *Nano Lett.* **2007**, *7*, 1251–1255.
54. McMahon, J. M.; Li, S.; Ausman, L. K.; Schatz, G. C. Modeling the Effect of Small Gaps in Surface-Enhanced Raman Spectroscopy. *J. Phys. Chem. C* **2012**, *116*, 1627–1637.
55. Chen, C. K.; Castro, A. R. B. d. Surface-Enchanced Second-Harmonic Generation. *Phys. Rev. Lett.* **1981**, *46*, 145–148.
56. Bao, H.; Bihr, T.; Smith, A.-S.; Klupp Taylor, R. N. Facile Colloidal Coating of Polystyrene Nanospheres with Tunable Gold Dendritic Patches. *Nanoscale* **2014**, 10.1039/C3NR04016J.
57. Wang, H.; Yan, E. C. Y.; Borguet, E.; Eisenthal, K. B. Second Harmonic Generation from the Surface of Centrosymmetric Particles in Bulk Solution. *Chem. Phys. Lett.* **1996**, *259*, 15–20.
58. Stöber, W.; Fink, A.; Bohn, E. Controlled Growth of Monodisperse Silica Spheres in the Micron Size Range. *J. Colloid Interface Sci.* **1968**, *26*, 62–69.
59. Duff, D. G.; Baiker, A. Preparation and Structural Properties of Ultrafine Gold Colloids for Oxidation Catalysis. *Stud. Surf. Sci. Catal.* **1995**, *91*, 505–512.
60. Schürer, B.; Elser, M. J.; Sternig, A.; Peukert, W.; Diwald, O. Delamination and Dissolution of Titanate Nanowires: A Combined Structure and *in Situ* Second Harmonic Generation Study. *J. Phys. Chem. C* **2011**, *115*, 12381–12387.
61. Schneider, L.; Schmid, H. J.; Peukert, W. Influence of Particle Size and Concentration on the Second Harmonic Signal Generated at Colloidal Surfaces. *Appl. Phys. B: Lasers Opt.* **2007**, *87*, 333–339.